BIOCHEMISTRY
including biophysical chemistry & molecular biology

ARTICLE

pubs.acs.org/biochemistry

Impact of BRCA1 BRCT Domain Missense Substitutions on Phosphopeptide Recognition

Nicolas Coquelle, Ruth Green, and J. N. Mark Glover*

Department of Biochemistry, School of Medicine, University of Alberta, Edmonton, Alberta T6G 2H7, Canada

Supporting Information

ABSTRACT: The BRCA1 BRCT domain binds pSer-x-x-Phe motifs in partner proteins to regulate the cellular response to DNA damage. Approximately 120 distinct missense variants have been identified in the BRCA1 BRCT through breast cancer screening, and several of these have been linked to an increased cancer risk. Here we probe the structures and peptide-binding activities of variants that affect the BRCA1 BRCT phosphopeptide-binding groove. The results obtained from the G1656D and T1700A variants illustrate the role of Ser1655 in pSer recognition. Mutations at Arg1699 (R1699W and R1699Q) significantly reduce peptide binding through loss of contacts to the main chain of the Phe(+3) residue and, in the case of R1699W, to a destabilization of the BRCT fold. The R1835P and E1836K variants do not dramatically reduce peptide binding, in spite of the fact that these mutations significantly alter the structure of the walls of the Phe(+3) pocket.

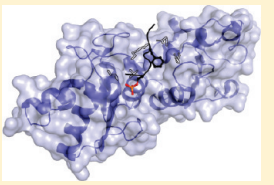

Widespread genetic testing for mutations in the breast cancer associated protein BRCA1 has revealed an unprecedented view of the range of genetic variability in this gene throughout the human population. To date, over 1600 distinct mutations have been uncovered within BRCA1 (collated in the Breast Cancer Information Core Database (BIC); http://research.nhgri.nih.gov/projects/bic). Unfortunately, efforts to classify the cancer risks associated with these mutations have been hampered by a lack of accurate family history and clinical data linking individual mutations to disease. Some of the most difficult variants to assess are the missense variants. 570 distinct missense variants have been detected throughout the 1863 codons of BRCA1; however, less than 2% of these have been conclusively associated with cancer. Intriguingly, all the disease-associated missense mutations occur within two domains: the N-terminal RING domain and the C-terminal BRCT domain, implicating these regions as critical for the tumor suppressor function of BRCA1.

BRCA1 plays an essential role in the response of cells to DNA damage, where it mediates complex protein−protein interactions that both regulate the cell cycle and promote DNA repair through homologous recombination in response to DNA damage.[1] Two domains are particularly critical in mediating protein−protein signaling events within the DNA damage response. The BRCA1 N-terminal RING domain, bound in a heterodimeric complex with the RING domain of BARD1, acts as an E3 ubiquitin ligase that likely ubiquitylates as yet undetermined targets.[2,3] The C-terminal pair of tandem BRCT repeats functions as a phosphopeptide binding module, selectively binding partner proteins such as the DNA helicase BACH1/FANCJ, the DNA resectioning factor CtIP, and DNA double strand break targeting protein, Abraxas.[4,5]

A number of functional and structural studies have provided details into the mechanism of phosphopeptide recognition employed by the BRCA1 BRCT domain. The two tandem repeats that make up the domain pack together in a head-to-tail manner that is characteristic of the packing seen in many other BRCT proteins that are involved in DNA damage signaling[6,7] (Figure 1A). The BRCA1 BRCT domain specifically binds phosphopeptide motifs containing a phosphoserine and a phenylalanine residue at the +3 C-terminal position.[4,5] N-terminal repeat provides a shallow pocket that recognizes the phosphoserine specifically over phosphothreonine[8] through electrostatic interactions between the phosphate group and ligands provided by Ser1655, Lys1702, and the main-chain NH of Gly1656[9−11] (Figure 1B). The critical phenylalanine residue is recognized by a largely hydrophobic groove formed at the interface between the two BRCT repeats. Interactions between the main chain of the +3 phenylalanine and Arg 1699 of BRCA1 help to position the +3 residue within this groove. BRCT repeats are a common protein module in many proteins involved in the DNA damage response, and the mechanism of phosphopeptide recognition employed by BRCA1 is likely conserved in several of these other proteins.[12,13]

Approximately 120 distinct missense variants have so far been uncovered within the BRCA1 BRCT repeats through breast cancer screening. To better understand the functional implications of these mutations, a variety of biochemical and cellular assays, as well as computational methods, have been developed to assess the impact of the individual mutations. Biophysical methods have been utilized to assess the effects of missense mutations on the folding of the BRCA1 BRCT domain; however, they often cannot be used because of an inability to produce and purify many of the different variants.[14−16] To counter this problem, other methods have utilized *in vitro* transcribed/translated proteins. The low levels of protein produced in this way, and possibly the

Received: March 14, 2011
Revised: April 6, 2011
Published: April 07, 2011

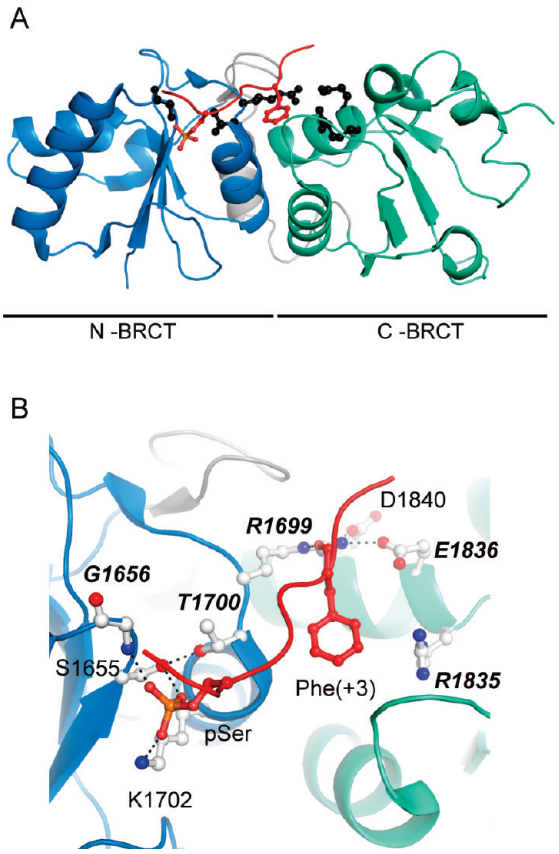

Figure 1. Structure of the wild-type BRCA1 BRCT domain complexed with a phosphopeptide. (A) Cartoon representation of the tandem BRCT repeats of BRCA1. The N-terminal BRCT repeat is colored blue, the C-terminal BRCT repeat is green, the inter-repeat linker is gray, and the bound phosphopeptide derived from BACH1 (residues 986−995) is red. The substituted residues analyzed in this study as well as the pSer and Phe(+3) side chains are highlighted as ball and sticks. (B) Close-up view of the BRCA1 phosphopeptide binding surface. Essential BRCA1 residues for peptide recognition as well as the peptide pSer and Phe(+3) residues are represented as ball and sticks.

presence of protein chaperones in the reticulocite extracts used, enable the production of essentially any variant. The folding stability of variants produced in this way have been assessed by their susceptibility to limited proteolysis,[6,17−19] and the phosphopeptide binding activities of the variants have been assessed through phosphopeptide pulldown studies.[11,17] Perhaps the most widely used cellular assay for the functional integrity of the BRCA1 BRCT domain is a transcriptional assay, derived from the finding that the BRCA1 BRCT domain can act as a transcription activation module in both human and yeast cells when tethered to a heterologous DNA binding domain.[20,21] While the *in vivo* relevance of this activity is still uncertain, the excellent correlation between cancer risk and the transactivation potential of the BRCA1 variant gives confidence that the transcription assay gives a meaningful readout of BRCA1 BRCT activity in a cellular context.[17] Experimental approaches have also been complemented by studies using bioinformatics analysis based on multiple sequence alignment,[22] structure prediction,[23,24] or multifactorial likelihood modeling in which available genetic data, co-occurrence, and predictive methods are combined.[25,26]

We recently completed a comprehensive analysis of the BRCA1 BRCT missense variant set, using proteolytic mapping, phosphopeptide binding, and transcriptional transactivation assays to assess the functional consequences of each mutation.[17] A comparison of these results with the available family history and clinical data for a subset of the variants revealed an excellent correlation, suggesting that these methods might be used as part of a cancer risk assessment strategy. The study revealed that of the 117 variants studied 42 showed little if any functional deficiencies, 50 showed strong functional deficiencies and might be associated with an increased cancer risk, while 25 showed functional activities intermediate between these two extremes. Several of the mutations targeted the essential peptide-binding surface of the BRCA1 BRCT domain. To understand the impact of this important class of variants and to uncover new principles of BRCT−phosphopeptide interactions, we have studied each of these six variants using a quantitative fluorescence polarization assay to determine the precise effect on peptide binding of each of these variants. The structural consequences of these variants were assessed through crystal structures of the variants, together with biophysical assessment of protein fold stability and computational studies. The results reveal in some cases an unexpected resilience of the phosphopeptide binding groove to mutation and provide a better basis to predict the functional consequences of these variants. This work provides new insight into phosphopeptide recognition of the BRCA1 BRCT domain that may be broadly applicable to this large family of proteins.

EXPERIMENTAL PROCEDURES

BRCT Purification. Variants characterized in this study were produced in pLM1-CD6[17] and were expressed in BL21-Gold cells for 18 h at 24 °C and purified as previously described.[6]

Fluorescence Polarization. The fluorescent BACH1-derived peptide was synthesized by Biomatik Corp. (Fluorescein-GGSRSTpSPTFNK-NH2). The peptide binding affinity was evaluated for each variant using different protein concentrations (from 20 nM to 500 μM) with a constant concentration of fluorescent peptide (100 nM) in a reaction volume of 20 μL. The fluorescein was excited at a wavelength of 458 nm, and the emitted fluorescence was recorded at 538 nm with a Perkin-Elmer Envision plate reader. The polarization change was plotted against the log of the protein concentration, and the K_d value was derived from the resulting curve. The experiments were performed in triplicate and carried out in parallel with wild-type BRCA1 BRCT.

Circular Dichroism. Proteins were incubated at 0.1 mg mL^{-1} in various guanidinium hydrochloride (GdmCl) concentrations (50 mM sodium phosphate pH 7.5, 400 mM NaCl) for 2 h at room temperature in duplicate. Far-UV CD spectra were recorded with a Jasco J-720 spectropolarimeter using a cell of 0.05 cm length from 250 to 210 nm. A wavelength step of 0.1 nm was used, and eight accumulations were carried out for each averaged spectra. Baseline correction was performed.

Crystallization. All the crystals were obtained using the hanging drop vapor diffusion method at room temperature. The crystals of variants T1700A, G1656D, R1699Q, and R1835P in their apo form were grown by mixing equal volumes of 18 mg mL^{-1} protein solution (2 μL) with well solution (0.6−1.0 M Li_2SO_4 pH 7.5−8.5, 5 mM $NiCl_2$ and 10 mM $CaCl_2$). Crystals appeared in the drops after 1 or 2 days and reached their maximum size within a week. Prior to cryztallization, E1836K variant (10 mg mL^{-1}) was mixed with a BACH1-derived decapeptide (Ac-SRSTpSPTFNK-NH2) at an equimolar concentration on ice. The crystallization conditions were derived from Clapperton et al.[9] Drops were composed of 2 μL of

Table 1. Data and Refinement Statistics

	G1656D (apo)	T1700A (apo)	R1699Q (apo)	R1835P (apo)	E1836K (holo)
resolution (Å)[a]	40−2.55 (2.55−2.60)	40−2.5 (2.57−2.50)	40−2.8 (2.85−2.80)	40 - 2.8(2.85-.280)	40−2.85 (2.90−2.85)
space group	$P6_122$	$P6_122$	$P6_122$	$P6_122$	$C222_1$
cell dimensions					
a (Å)	114.87	114.38	114.62	114.95	115.82
b (Å)	114.87	114.38	114.62	114.95	131.05
c (Å)	122.11	122.32	122.11	121.95	180.84
completeness (%)	98.1 (99.4)	99.1 (99.8)	98.8 (99.4)	97.5 (97.6)	96.1 (73.6)
$\langle I/\sigma I \rangle$	18.4 (3.1)	14.7 (2.6)	16.6 (3.0)	16.3 (2.2)	17.8 (2.2)
redundancy	4.8 (4.9)	3.5 (3.6)	4.7 (4.5)	3.1 (3.1)	4.4 (3.5)
R_{sym}	0.051 (0.479)	0.048 (0.487)	0.057 (0.502)	0.059(0.588)	0.058 (0.487)
resolution (Å)	40−2.55	40−2.5	20−2.8	40−2.8	45−2.85
no. of subunits	1	1	1	1	4
R_{work}/R_{free}	0.238/0.261	0.235/0.274	0.228/0.270	0.233/0.281	0.220/0.266
no. of atoms					
protein	1630	1621	1614	1636	6617
peptide	0	0	0	0	198
water	29	14	13	8	16
nickel	1	1	1	1	0
sulfate	5	5	5	5	0
overall *B* factor (Å^2)	80.3	84.5	92.3	96.2	97.2
rmsd					
bond length (Å)	0.008	0.008	0.008	0.008	0.007
bond angle (deg)	1.17	1.14	1.18	1.12	1.08
Ramachandran[b]					
preferred (%)	95.1	93.6	94.0	88.8	95.1
allowed (%)	4.9	4.4	6.0	10.7	4.7
disallowed (%)	0.0	0.0	0.0	0.5	0.2

[a] Values in parentheses refers to highest resolution shell. [b] As reported by Molprobity Server (http://molprobity.biochem.duke.edu/).

protein solution and 2 μL of 50 mM MES pH 6.5, 26% PEG 8000, 0.15 mM $(NH_4)_2SO_4$. Cocrystallization was also carried out for the other variants under these conditions, but no crystals were obtained.

Data Collection and Processing. Crystals were soaked in a cryoprotectant solution (well solution complemented with 20−25% glycerol) for 1−5 min and then flash-cooled in liquid nitrogen. All the data were recorded at 100 K on the Canadian Light Source 08ID-1 beamline, with the exception of R1699Q data, collected on ALS beamline 12.3.1. Diffracting frames were indexed and integrated using XDS[27] and were scaled and merged with XSCALE and XDSCONV (Table 1).

Model Building and Refinement. The different structures were solved using the molecular replacement method (resolution range 40−3 Å) with the software PHASER.[28] The initial search model was a previously solved BRCA1 BRCT structure (PDB code 1n5o). Crystals of the different apo variants (R1699Q, T1700A, G1656D, and R1835P) grew in the space group $P6_122$ with one molecule in the asymmetric unit. Electron density for the substituted amino acid was clear in the $mF_o - DF_c$ maps (see Figure S1). Refinement of the models was performed with Phenix:[29] initial rigid-body refinement and simulated annealing was followed by cycles of energy minimization, individual isotropic temperature factor refinement, and TLS refinement. Five TLS groups were defined per molecule (two for the N-BRCT, one for the linker region, and two for the C-BRCT) using the TLSMD server.[30,31] Model refinement was interspersed with sessions of model rebuilding using the program Coot.[32] In these models, a strong peak was observed in the $mF_o - DF_c$ Fourier difference map between two molecules of the crystal. A nickel ion was modeled at this position and is coordinated to residues His1805 and His1673 from a symmetry mate as well as two water molecules.[6,33]

The E1836K variant bound to a decapeptide crystallized in space group $C222_1$ with four complexes in the asymmetric unit. Model building and refinement were carried out as described above with NCS restraints. The solvent content in this crystal is about 75%. Poorer quality electron density was associated with chains C and D compared to chains A and B, probably due to a poorer packing of these chains in the crystal lattice. 4-fold NCS averaging was used to improve maps in the areas of weak density in chains C and D corresponding to the linker and the $\beta3-\alpha2$ and $\beta2'-\beta3'$ loops. The positive electron density of the $mF_o - DF_c$ map contoured at 3σ was not good enough to completely model the side chain of Lys1836. A simulated-annealing composite omit map was therefore calculated with CNS 1.21,[34] and the resulting $2mF_o - DF_c$ map clearly indicates density for the side chain of the lysine in monomers A, B, and C, but not in monomer D (Figures S1E, S1F, and S1G). The occupancies of the modeled peptides were refined.

The geometry of the refined models was checked with the molprobity server.[35] A summary of final models statistics is provided in Table 1. The coordinates as well as structure factors have been deposited in the Protein Data Bank (accession code 3pxa for G1656D, 3pxb for T1700A, 3pxc for R1699Q, 3pxd for R1835P, and 3pxe for E1836K bound to a phosphopeptide). PyMOL was

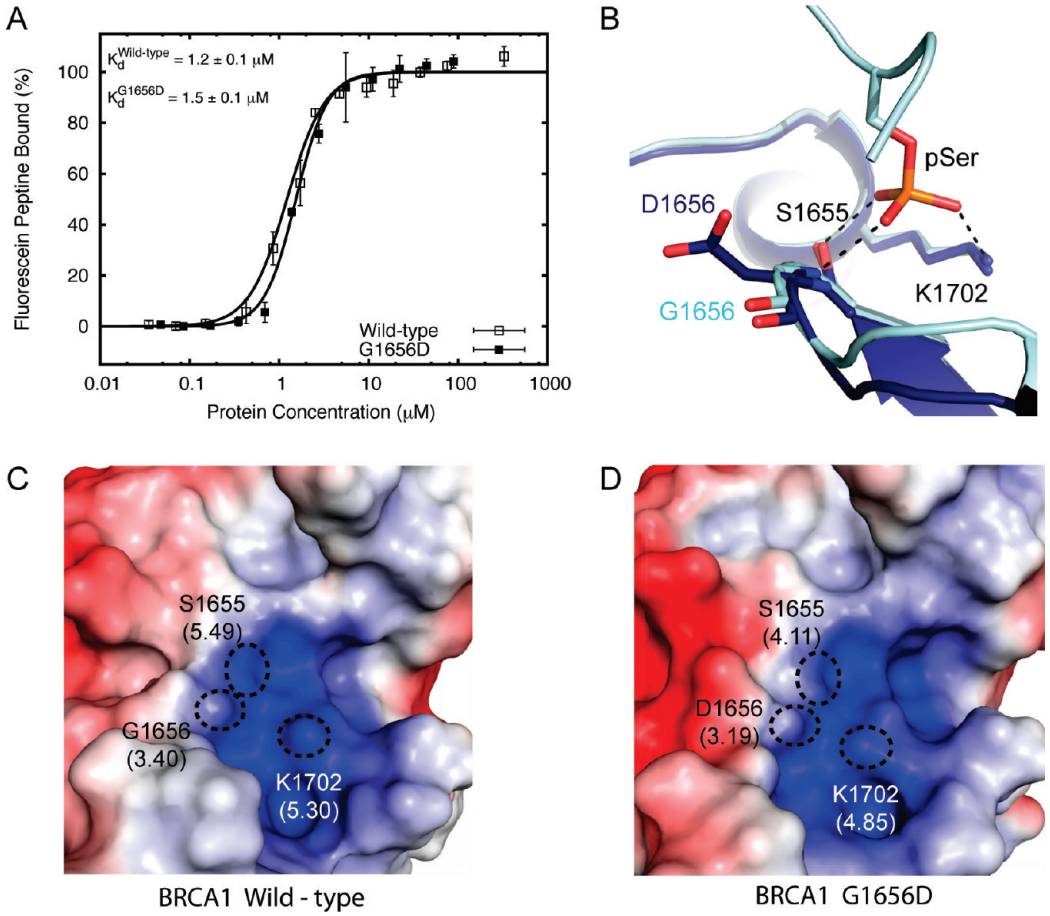

Figure 2. Phosphopeptide binding and structural comparison of the wild-type BRCA1 BRCT and the G1656D variant. (A) Assessment of the phosphopeptide binding properties of the wild-type BRCA1 BRCT (open squares) and the G1656D variant (filled squares) using a fluorescence polarization (FP) assay. (B) Cartoon overlay of wild-type (cyan) and G1656D variant (dark blue) BRCT domain. Residues involved in phosphate recognition are represented as sticks. (C, D) Representation of electrostatic potential of wild-type (C) and G1656D variant (D) BRCT domain. The surface of atoms that directly binds the phosphoserine is contoured (dashed lines), and the corresponding electrostatic potential is indicated in parentheses (in kT e^{-1}).

used to produce all the figures (The PyMOL Molecular Graphics System, Version 1.2r3pre, Schrödinger, LLC). The electrostatic potential was calculated with APBS[36] at 300 K.

Molecular Dynamics Simulations. The crystal structure of the wild-type BRCT domain complexed with a phosphopeptide[9] (pdb code 1t15) and the crystal structure of the missense variants T1700A (pdb code 3pxb) were used as starting points for the simulations. The apo form of wild-type BRCT was simulated from the same initial crystal structure (pdb code 1t15) in which the phosphopeptide was removed. Each protein was first submitted to energy minimization in vacuo and was subsequently solvated in a 10.27 nm side-length cubic box. The distance of the protein from the box walls was at least 15 nm. The system was neutralized by addition of the appropriate number of counterions, energy minimized, and equilibrated at 300 K. For each system, four 10 ns simulations were performed with different initial velocities. GROMACS package[37] was used to perform MD simulations using GROMOS 53a6 force field[38] that we modified to contain phosphoserine residue. A constant temperature of 300 K was maintained using a Berendsen thermostat with a coupling time of 0.1 ps.[39] A Berendsen barostat was used to keep pressure at 1 bar with τ_p = 1.0 ps and a compressibility of 4.5 × 10^{-5} bar^{-1}.[39] Electrostatic interactions were calculated using the particle mesh Ewald method.[40,41] Bond lengths were restrained with the LINCS algorithm,[42] allowing a 2 fs integration step. Coordinates of the system were saved every 1 ps.

RESULTS

Selection of BRCA1 BRCT Missense Variants for Detailed Structure/Function Analysis. Our previous analysis of the structural and functional consequences of missense mutations in the BRCA1 BRCT domain uncovered an intriguing class of defective variants in which folding of the protein was not destabilized as assayed by limited proteolysis.[17] We reasoned that the functional defects associated with these variants likely were due to localized changes of the phosphopeptide binding groove. Indeed, the variants M1775R and M1775K fall into this class, and previous structural and peptide binding studies revealed that conformational changes associated with these mutations block the +3 specificity pocket of this surface.[11,19,43] Six additional mutations were identified in or near the phosphopeptide binding groove: G1656D, R1699W, R1699Q, T1700A, R1835P, and E1836K. Three missense variants, R1699Q, R1699W, and T1700A, were scored as "strong functional effect" in Lee et al.'s study as they exhibited compromised activities in all the functional assays. The other variants, G1656D, R1835P, and E1836K,

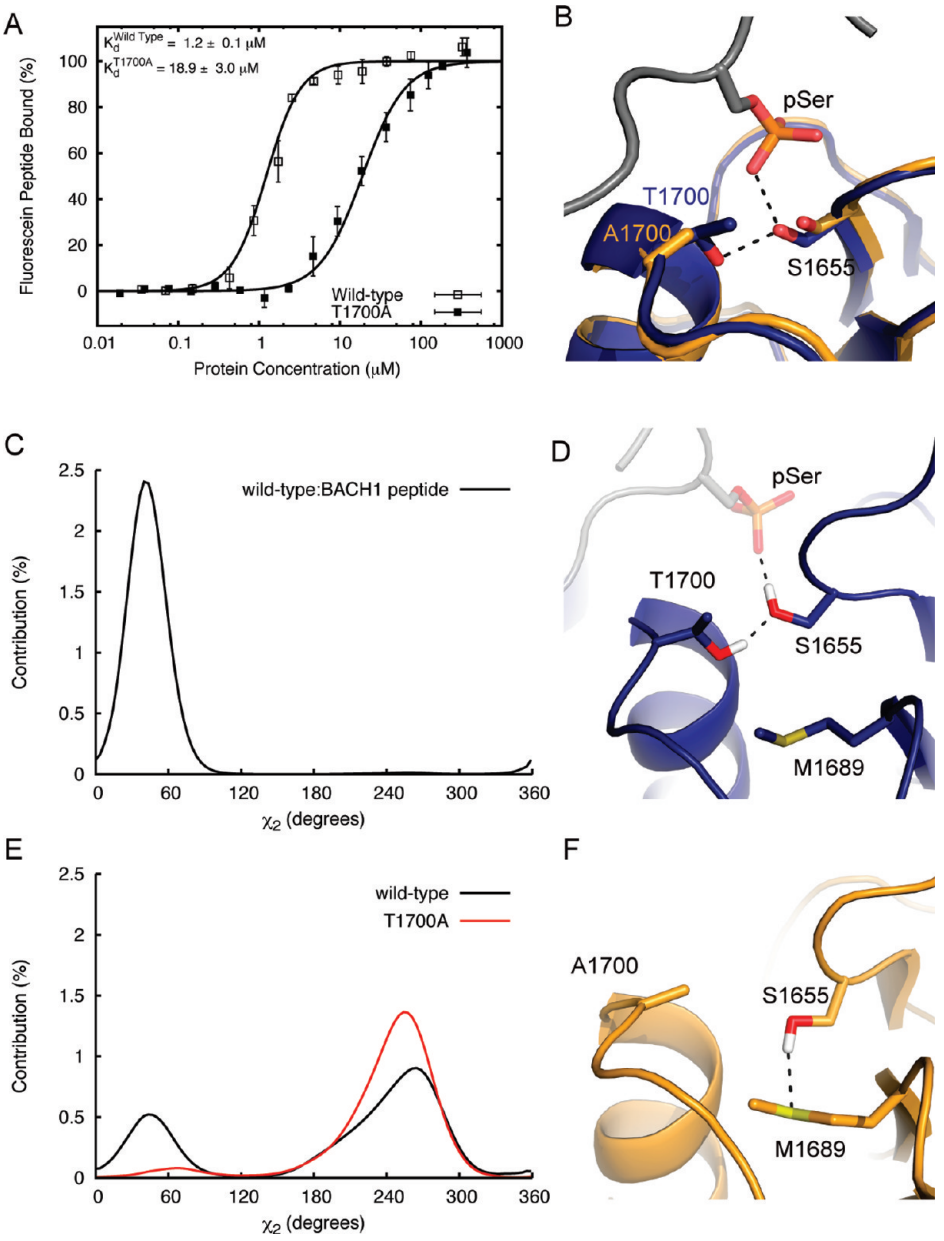

Figure 3. T1700A substitution reduces phosphopeptide binding affinity due to enhanced rotational freedom of a key phosphate ligand. (A) FP experiments comparing the ability of BACH1-derived decapeptide to bind to BRCA1 BRCT wild-type (open squares) and the T1700A variant (filled squares). (B) Superimposition of BRCA1 BRCT structure bound to a phosphopeptide (pdb entry 1t15) in gray (phosphopeptide) and blue (BRCT) with the structure of the T1700A variant in orange. (C) Ser1655 χ_2 angular distribution obtained from an MD simulation of the wild-type BRCA1 BRCT bound to a phosphopeptide. (D) Snapshot extracted from the wild-type BRCA1 BRCT−phosphopeptide MD simulation. Important hydrogen bonds are shown as dashed lines. The phosphopeptide is transparent as this Ser 1655 conformation is also commonly populated in a simulation of the unbound form of the wild-type BRCA1 BRCT. (E) Ser 1655 χ_2 angular distribution obtained from the apo wild-type BRCA1 BRCT simulation (black line) and from the T1700A variant simulation (red line). (F) Snapshot extracted from T1700A variant simulation. In this conformation, the Ser1655 side chain hydroxyl is pointing away from the peptide-binding groove and may interact with Met1689.

however, showed poor agreement between the different functional assays, complicating assessment of the true impact of these mutations. To further probe the functional defects associated with these variants, we expressed and purified each variant for detailed structural and functional analyses.

G1656D: Addition of a Negative Charge Close to the Phosphoserine Recognition Pocket. The Gly1656 main-chain NH provides a critical ligand that binds the phosphate of the target phosphopeptide. Mutation of this invariant residue to aspartic acid could be expected to block phosphopeptide binding through a steric clash, an electrostatic repulsion of the aspartate with the phosphate, or a conformational effect related to the restricted main-chain geometries available to Asp compared to Gly. The effect of this amino acid substitution on phosphopeptide recognition was tested using a fluorescence polarization (FP) assay, which has proven to be a highly sensitive method to assess quantitative changes in BRCT−phosphopeptide binding affinities.[33] The binding affinity of the G1656D variant to a fluorescein-labeled

dx.doi.org/10.1021/bi2003795 |*Biochemistry* 2011, 50, 4579–4589

BACH1 decapeptide was compared to that of the wild-type BRCA1 BRCT domain (Figure 2A). Surprisingly, the K_d values for the wild-type and the G1656D variant are in the same narrow range, 1.2 ± 0.1 and 1.5 ± 0.1 μM, respectively, indicating that this mutation has little if any impact on phosphopeptide binding.

To understand how this variant is able to bind phosphopeptide, the X-ray crystal structure of G1656D was determined at 2.55 Å resolution (Table 1). The overall folding is identical to the wild type, and the side chain of the aspartic residue at position 1656 could easily be modeled in the electron density of the $mF_o - DF_c$ map (Figure S1A). A comparison of this model to the structure of wild-type BRCT bound to a phosphopeptide reveals that the aspartic acid side chain is oriented away from the phosphate binding pocket and does not induce any major structural reorganization of the protein backbone (Figure 2B).

The effect of the extra negative charge on the electrostatic potential of the phosphate recognition pocket was analyzed with the program APBS.[36] The calculation was performed using a 0.3 Å grid over the peptide-binding surface to allow quantitative comparisons between the wild-type and G1656D variant. While the electrostatic potential of the variant is negative near the carboxylate group of the introduced aspartate side chain, the potential throughout the phosphate binding pocket remains positive, and little difference is observed in the region of the three phosphate ligands: the mainchain NH of Gly/Asp1656; the hydroxyl group of Ser1655; and the side chain amino group of Lys1702 (Figure 2C, D). The most significant change in the electrostatic potential of these ligands is observed near Ser1655 (reduction of 25%), whereas reduction of the positive potential is less pronounced near residue 1656 and Lys1702 (reduction of 6.1 and 8.5%, respectively). These results suggest that the electrostatic potential of the Ser1655 ligand may be less critical for phosphate binding, compared to the residue 1656 and Lys1702 ligands.

T1700A: Influence of a Hydrogen Bond on the Ser 1655 Conformational Landscape. The crystal structure of wild-type BRCA1 BRCT domain indicates that the orientation of the Ser1655 side chain is maintained through a hydrogen bond with Thr1700 in a conformation that facilitates hydrogen bonding of the Ser1655 hydroxyl group with the phosphate (Figure 1B). To assess the impact of the T1700A substitution on phosphopeptide recognition, the ability of this variant to bind a BACH1-derived peptide was examined using FP spectroscopy (Figure 3A). The results indicate that the BACH1-derived decapeptide binds to T1700A with a K_d of 18.9 ± 3.0 μM, a 15-fold reduction compared to wild type.

To investigate the structural properties that could account for this significant change in peptide binding affinity, the crystal structure of T1700A was determined at 2.5 Å resolution. Comparison of this structure with that of the wild-type reveals only a slight reorientation of the Ser1655 side chain; however, the resolution of this structure is not sufficient to assign the orientation of the Ser1655 hydroxyl (Figure 3B and Figure S1B). To assess the possible effect on this mutation on Ser1655 hydroxyl orientation, we carried out molecular dynamic simulations of the T1700A variant and compared the results to parallel calculations with the wild-type BRCA1 BRCT, both free and bound to phosphopeptide. Dynamic properties of the Ser1655 side chain were inferred from a series of 40 000 structural snapshots taken at 1 ps intervals along the MD trajectories, and the two serine side-chain dihedral angles, χ_1 (N−Cα−Cβ−Oγ) and χ_2 (Cα−Cβ−Oγ−Hγ), were calculated. The χ_1 distributions indicate a very low flexibility, centered around 190°, which is not affected by the T1700A substitution (Figure S2A). In contrast, major discrepancies are observed in the χ_2 angular distributions. For simulations of the wild-type bound to a BACH1 phosphopeptide, the χ_2 angular distribution is centered around +40°, maintaining

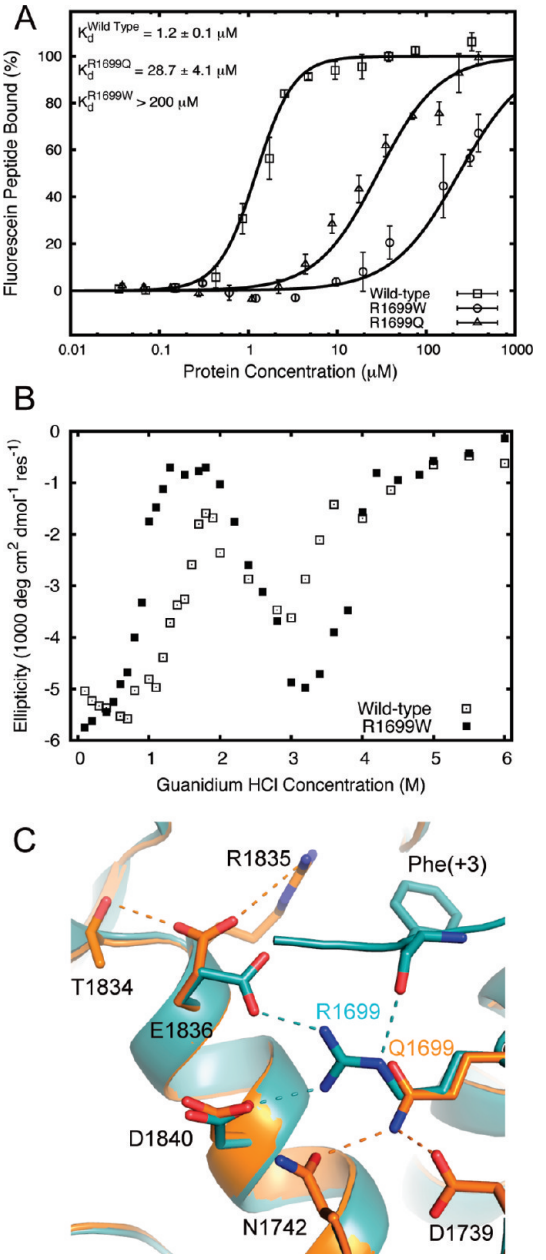

Figure 4. Effect of different amino acid substitutions at position 1699 on BRCT structure, stability, and interactions with a BACH1 phosphopeptide. (A) FP experiments were used to compare the affinity of wild-type BRCT domain (open squares), the R1699Q (open triangles), and the R1699W variants (open circles) to bind a BACH1 derived phosphopeptide. (B) Comparison of GdmCl denaturation curves of wild-type BRCT (open squares) and the R1699W variant (filled squares) followed by CD spectroscopy monitored at 222 nm. (C) Overlay of wild-type BRCA1 BRCT domain (cyan, pdb entry 1t15) and the R1699Q variant (orange). Residues interacting with wild-type Arg1699 or the variant Gln1699 are represented as sticks as well as the Phe(+3) residue of the phosphopeptide. Important hydrogen-bonding interactions are shown as dashed lines (cyan for wild type, orange for R1699Q).

dx.doi.org/10.1021/bi2003795 |*Biochemistry* 2011, 50, 4579–4589

hydrogen bonds with both the phosphate group and Thr1700 throughout the entire simulation (Figure 3C,D and Figure S2B). For the simulated apo wild-type and T1700A systems, the χ_2 values are more dispersed. Two major χ_2 orientations are observed in the wild-type simulation (Figure 3D,E). In one, the hydrogen atom is oriented toward the peptide binding groove, similar to the orientation observed in the peptide-bound simulation (23.3% of total conformations), while in the other, χ_2 is between 220° and 280°, orienting the hydroxyl group away from the phosphate binding pocket and allowing a possible hydrogen bond with the sulfur atom of Met 1689. The hydrogen bond between Thr1700 and Ser1655 is observed in 46% of saved snapshots (Figure S2C) and correlates with orientation of the Ser1655 hydroxyl group toward the peptide-binding groove. For the T1700A system, the Ser1655 Hγ is very rarely oriented toward the peptide-binding groove (only 3.3% of all simulated conformations) and is mostly in the opposite direction where it can interact with Met1689 (Figure 3F). This suggests that loss of the hydrogen bond between Thr1700 and Ser1655 in T1700A drastically changes the conformational space sampled by the Hγ diminishing the number of orientations competent for phosphate recognition. This may explain the difference observed in peptide affinity between the wild-type and the T1700A missense variant.

Analysis of Missense Variants at Position 1699. Arg1699 plays an important role in phosphopeptide recognition through its interactions with the peptide main chain at the +3 position that likely draw the +3 side chain into the BRCT specificity pocket (Figure 1B). Interestingly, three missense variants have been uncovered at this position: R1699L, R1699Q, and R1699W. Peptide recognition was analyzed for the R1699Q and R1699W variants with the FP assay (Figure 4A). For the missense variant R1699Q, the observed K_d value was 28.7 ± 4.1 μM, a 24-fold reduction compared to wild type. For the second variant R1699W, binding was much weaker, and the K_d could not be precisely determined (>200 μM), corresponding to at least a 160-fold reduction in affinity compared to wild type. Similar results for these variants have been obtained utilizing a different phosphopeptide in a recent study.[15] Thus, while both variants display significant defects in phosphopeptide binding affinities, the R1699W variant appears to be more deleterious.

Limited proteolysis suggested that R1699W is properly folded;[17] however, we noticed that this variant tends to aggregate when concentrated, suggesting a folding defect that might not be detected by the proteolysis assay. To probe the thermodynamic stability of this variant, guanidinium hydrochloride (GdmCl) denaturation profiles, monitored with circular dichroism spectroscopy (CD) at 222 nm, were compared between R1699W and the wild-type BRCT domain. The unusual shape of the denaturation curves represented in Figure 4B are similar to those previously obtained[14,15] and indicate that the BRCT domain unfolds via an aggregation-prone intermediate. Here, a first transition is observed for the wild type between 1 and 2 M GdmCl and likely corresponds to the formation of the aggregation-prone intermediate. This first transition is shifted toward lower GdmCl concentrations for R1699W, suggesting a decreased free energy of unfolding between the folded state and the intermediate. Around 3 M GdmCl, a second minima is observed, corresponding to the intermediate. The negative ellipticity is greater for the missense R1699W, suggesting a more structured intermediate. At higher GdmCl concentrations, the ellipticity increases as the unfolding of the intermediate occurs. This transition is shifted toward higher GdmCl concentrations for the missense R1699W. This would indicate an increased free energy of unfolding between the intermediate and the unfolded state. Thus, at least part of the binding defect associated with the R1699W mutation is likely due to protein destabilization. In addition, we predict that the introduction of the bulky hydrophobic Trp at position 1699 will likely interfere with docking of the peptide +3 position into the BRCT peptide-binding groove. Unfortunately, we have not been able to grow crystals of this variant of sufficient quality for structure determination to directly visualize any structural changes induced by this substitution.

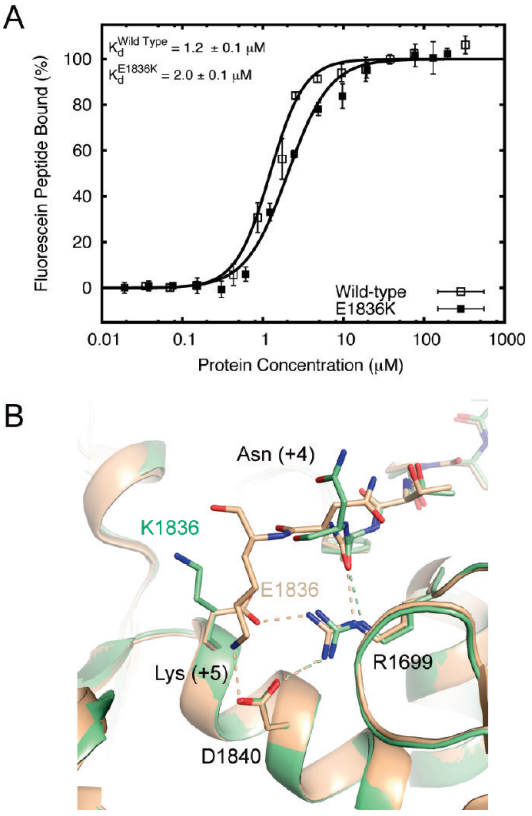

Figure 5. Functional and structural impact of a charge swap in the vicinity of Arg1699. (A) Determination of the binding affinities of wild-type BRCA1 BRCT (open squares) and the E1836K variant (filled squares) for a BACH1-derived phosphopeptide using FP. (B) Superimposition of wild-type BRCA1 BRCT (pdb code 1t15, orange) and the E1836K variant (green), both bound to a BACH1 phosphopeptide. Residues in the vicinity of the substitution are shown as sticks, and important hydrogen bonds are represented as dashed lines.

To uncover the molecular characteristics responsible for the decrease in peptide binding affinity of the R1699Q variant, the structure of this variant was determined at 2.8 Å resolution. The glutamine residue at position 1699 adopts a very similar orientation to that of the arginine in the wild-type structure (Figure 4C and Figure S1C). The glutamine side chain is positioned so that the side chain NH2 hydrogen bonds with Asp1739 and Asn1742, interactions not observed in the wild-type structure. Because the introduced glutamine is shorter than the arginine side chain, the interactions with Asp1840 and Glu1836 are lost, and Glu1836 adopts a different rotamer in response to the substitution. The impact of the positioning of Gln1699 is that the side-chain carbonyl is directed toward the peptide binding cleft, such that it would clash with the main-chain carbonyl at the peptide +3 position, providing an explanation for its decreased peptide affinity.

dx.doi.org/10.1021/bi2003795 |*Biochemistry* 2011, 50, 4579–4589

E1836K: A Charge Swap Close to the Binding-Site Residue R1699. In wild-type BRCA1, the highly conserved residue, Glu1836, forms a salt bridge with the Arg1699 side chain, likely helping to position the Arg guanidinium group to bind to the peptide main chain (Figure 1B). We expected that the Glu-Lys substitution at this position would therefore impact peptide binding, and this prediction was tested with the FP assay. Surprisingly, the K_d of the E1836K variant was 2.0 ± 0.1 μM, only ~2-fold reduced compared to wild type. To understand the molecular binding mode in the variant E1836K, the crystal structure of this variant complexed with a BACH1-derived phosphopeptide was determined at 2.85 Å resolution. In three of the four complexes in the crystallographic asymmetric unit, the introduced lysine side chain could be modeled. A similar conformation around the site of substitution is observed in each of these three complexes that accommodates the charge swap at position 1836 (Figure 5B and Figure S1E−G). In these complexes, Lys1836 is directed away from Arg1699, and the peptide at position +4 shifts to accommodate this change (Figure 5B). The Lys(+5) side chain of the peptide could not be modeled in any of the complexes and is likely disordered. This model provides a molecular basis of peptide binding mode in missense variant E1836K and reveals how the different positive charges from the protein and the peptide can be accommodated to maintain a peptide binding affinity similar to the wild type.

R1835P: Remodeling of the Phe(+3) Binding Pocket. The interface between N- and C-terminal BRCT repeats (Figure 1) forms a largely hydrophobic cleft that recognizes the Phe(+3) residue of the peptide. The lower surface is composed of Met1775, Leu1701, Leu1839, and Phe1704, whereas residues Asn1774 and Arg1835 define the side of this pocket (Figure 6A). Mutation of the arginine at position 1835 to proline has been uncovered from breast cancer screening, and we used the FP assay to determine the effect of this substitution on peptide binding (Figure 6B). The R1835P variant exhibits a small but significant 3-fold decrease in phosphopeptide affinity compared to wild-type BRCT domain (K_d = 3.6 ± 0.6 μM). To gain structural insight into this binding defect, the crystal structure of the R1835P variant was determined at 2.8 Å resolution (Figure 6C, Figure S1D, and Table 1). The conformational restriction of the proline at position 1835 leads to a small shift in the main-chain conformation but is otherwise well accommodated at the N-terminus of α3′. The replacement of the long arginine side chain with the more compact proline opens one side of the Phe recognition pocket and also appears to induce a conformational change in the α1′−β1′ loop that is most significant near Asn1774 (Figure 6C). This partial remodeling of the hydrophobic pocket may therefore explain the decrease in peptide affinity observed for the R1835P variant.

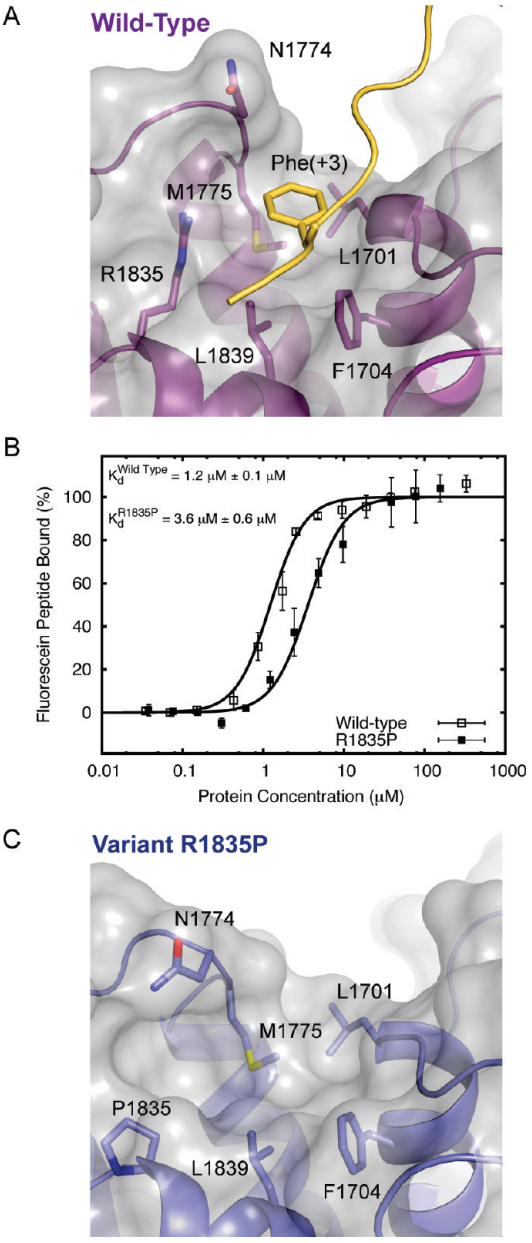

Figure 6. Alteration of the hydrophobic Phe(+3) recognition pocket in the R1835P Variant. (A) Close-up view of the Phe(+3) recognition pocket of the wild-type BRCA1 BRCT. Residues that comprise the pocket are shown as sticks with the van der Waals surface in gray. The phosphopeptide with Phe(+3) side chain in sticks is displayed in orange. (B) FP experiments were used to assess the affinity of wild-type BRCA1 BRCT (open squares) and the R1835P variant (filled squares) for the BACH1 phosphopeptide. (C) Close-up view of the Phe(+3) recognition pocket in the R1835P variant. Residues that comprise the pocket are shown as sticks.

DISCUSSION

Our previous study of the functional consequences of a large set of BRCA1 BRCT variants revealed an intriguing subset of the variants that were stably folded but nevertheless exhibited significantly reduced function in both peptide binding and transcriptional assays, likely through a direct effect on the phosphopeptide binding surface.[17] The phosphopeptide recognition surface of BRCA1 can be subdivided into two regions: one responsible for recognition of the target phosphoserine residue and the second responsible for recognition of the target phenylalanine residue at the +3 position with respect to the phosphoserine. Here we present a detailed analysis of the structural and functional properties of six variants that target these specific regions.

Two variants were studied that directly impact the phosphoserine recognition surface: G1656D and T1700A. Both Gly1656 and Thr1700 are strictly conserved in BRCA1, and it was therefore surprising that only the T1700A but not the G1656D mutation reduces peptide-binding affinity. The G1656D mutation introduces a negatively charged residue near the phosphate-

binding pocket that imposes a significant decrease in the electrostatic potential at one of the key phosphate ligands, the Ser1655 hydroxyl. While this might be expected to negatively effect phosphate binding, recent high-resolution structural studies of *S. pombe* Brc1 bound to a target phosphopeptide provide a possible explanation for the phosphopeptide binding activity of this variant.[44] Differences in the bond lengths between the phosphate oxygens and their coordinating ligands in the Brc1 structure indicate that the phosphate oxygens bound to the mainchain NH and lysine amino group (positions 1656 and 1702 in BRCA1) bear the majority of the negative charge, while the phosphate oxygen bound to the serine hydroxyl is predominantly neutral.[44] Such a binding mode would accommodate a reduction in the electrostatic potential at the Ser1655 hydroxyl and could therefore explain the lack of binding defect observed for the G1656D variant. Nevertheless, the Ser1655 hydroxyl is still a critical binding ligand, since the shift in its orientation induced by the T1700A substitution significantly reduces binding. Taken together, this indicates that the Ser1655 hydroxyl group functions primarily as a hydrogen bond donor in phosphate recognition but that its contributions to recognition through an electrostatic effect are limited.

Several variants were also studied that potentially impact the +3 specificity pocket: R1699W, R1699Q, R1835P, and E1836K. Arg1699 is absolutely conserved in BRCA1 and positions the peptide +3 residue in the specificity pocket through a pair of hydrogen-bonding interactions. The Arg1699 guanidinium group binds the peptide main chain carbonyl, while the main chain carbonyl of Arg1699 binds the main chain NH of the peptide +3 residue. The R1699W variant is unable to bind phosphopeptide, likely due to the perturbation of these interactions, as well as an overall destabilization of the protein fold, consistent with recent results from other groups.[15] In contrast, the R1699Q substitution is more conservative and does not appear to destabilize protein folding to a significant degree. It is able to bind the BACH1 phosphopeptide, albeit with significantly reduced affinity, probably due to the loss of hydrogen-bonding potential between the glutamine side chain and the peptide backbone. Interestingly, arginine residues are conserved at analogous positions in other peptide-binding BRCT proteins such as MDC1, BRC1, Crb2, and the TopBP1 7/8 tandem repeat, where they contact the peptide backbone at the peptide +3 position. The analogous arginine in MDC1 (Arg1933) plays a particularly important role in the selective recognition of the phosphorylated tail of γH2AX, where it forms a dual salt bridge with the peptide C-terminus at the +3 position.[45] Amidation of the γH2AX C-terminal carboxylate abrogates MDC1 recognition, underlining the importance of the dual salt bridge in the binding process.[46] Likewise, the BRCA1 BRCT domain also preferentially binds phosphopeptide targets in which the +3 residue terminates the chain (such as in the double strand break associated protein, Abraxas).[33] One of the tandem BRCT domains that does not contain an arginine at this position is the BRCA1 partner protein, BARD1. While early studies suggested this protein could bind phosphopeptides,[47] more recent studies have not replicated these initial findings[48,49] and have suggested that peptide binding may require elevated pH.[50] The structure of this tandem BRCT repeat domain reveals a very similar overall structure to BRCA1, with an intact phosphate binding pocket, but a serine in place of the conserved arginine, which would significantly impact the way in which this domain could contact target peptides.

Arg1699 is held in place through salt bridging interactions with Glu 1836 and Asp 1840 that span the interface between the N- and C-terminal BRCT repeats and likely stabilize Arg1699 for phosphopeptide recognition. Glu1836 is conserved in BRCA1 as well as MDC1. The E1836K mutation was expected to perturb this interaction network, and it was therefore surprising that this variant does not dramatically reduce phosphopeptide binding. The reason for this is revealed in the crystal structure of this variant bound to the BACH1 phosphopeptide, in which Arg1699 remains in place for interactions with the peptide backbone, likely through its stabilizing salt bridge to Asp 1840. The substituted residue, Lys1836, adopts an orientation in which it swings away from Arg1699, thereby avoiding a potentially detrimental electrostatic clash.

The final variant, R1835P, directly affects the pocket that binds the phenylalanine side chain at the peptide +3 position. Other well-studied variants, M1775R and M1775K, disrupt this pocket and are linked to an increased cancer risk.[19,43] Met1775 occupies the floor of this pocket, and its mutation to arginine or lysine leads to a conformational change so that substituted positively charged side chain fills the specificity pocket, blocking phosphopeptide binding. Arg1835 is largely conserved in mammalian BRCA1 and forms one side of the recognition pocket. Mutation of this residue to a proline essentially removes one face of the recognition pocket and results in small conformational changes in the vicinity of the pocket. In spite of these changes, this mutation leads to only a very modest decrease in peptide binding affinity, suggesting that Arg1835 contributes little to the recognition of the peptide +3 phenylalanine. Both rat and murine BRCA1s contain a tryptophan at this position that provides a more hydrophobic environment for the bound phenylalanine residue.

Taken together, this work suggests that the critical phosphopeptide binding surface of BRCA1 can be particularly sensitive to subtle missense mutations. Interestingly, while we have focused on missense variants that occur in or near this surface, missense substitutions that occur relatively far from the phosphopeptide binding surface can also exert subtle conformational effects that significantly impact function. The best-studied example to date is V1809F. Val1809 is positioned within the protein hydrophobic core, and the structure of the V1809F variant reveals a concerted conformational change in which the large phenylalanine residue drives the adjacent Leu1780 into a different conformation, which in turn induces a conformational change in Met1775 that blocks the +3 specificity pocket.[11] The detailed analysis of the BRCA1 variants ultimately can provide important new insights into the functional impact of these variants, which potentially could help define the cancer risks associated with these otherwise largely uncharacterized variants.

■ ASSOCIATED CONTENT

Supporting Information. Fourier difference maps for the different variants (Figure S1); some properties of residues S1655 extracted from molecular dynamics simulations (Figure S2). This material is available free of charge via the Internet at http://pubs.acs.org.

■ AUTHOR INFORMATION

Corresponding Author

*E-mail: mark.glover@ualberta.ca. Tel: 780-492-2136. Fax: 780-492-0886.

Funding Sources

This work was supported by a grant from the Canadian Cancer Society to J.N.M.G. J.N.M.G. also acknowledges the support of

the Howard Hughes Medical Institute International Scholar Program.

■ ACKNOWLEDGMENT

We thank P. Grochulski (Canadian Light Source, Saskatoon, SK) and J. Holton (Advandced Light Source, Berkeley, CA) for help with diffraction data collection. We also thank WestGrid and AICT from University of Alberta for access to computational ressources.

■ REFERENCES

(1) Huen, M. S., Sy, S. M., and Chen, J. (2010) BRCA1 and its toolbox for the maintenance of genome integrity. *Nat. Rev. Mol. Cell Biol. 11*, 138–148.

(2) Brzovic, P. S., Rajagopal, P., Hoyt, D. W., King, M. C., and Klevit, R. E. (2001) Structure of a BRCA1-BARD1 heterodimeric RING-RING complex. *Nat. Struct. Biol. 8*, 833–837.

(3) Brzovic, P. S., Keeffe, J. R., Nishikawa, H., Miyamoto, K., Fox, D., III, Fukuda, M., Ohta, T., and Klevit, R. (2003) Binding and recognition in the assembly of an active BRCA1/BARD1 ubiquitin-ligase complex. *Proc. Natl. Acad. Sci. U.S.A. 100*, 5646–5651.

(4) Yu, X., Chini, C. C., He, M., Mer, G., and Chen, J. (2003) The BRCT domain is a phospho-protein binding domain. *Science 302*, 639–642.

(5) Manke, I. A., Lowery, D. M., Nguyen, A., and Yaffe, M. B. (2003) BRCT repeats as phosphopeptide-binding modules involved in protein targeting. *Science 302*, 636–639.

(6) Williams, R. S., Green, R., and Glover, J. N. (2001) Crystal structure of the BRCT repeat region from the breast cancer-associated protein BRCA1. *Nat. Struct. Biol. 8*, 838–842.

(7) Glover, J. N., Williams, R. S., and Lee, M. S. (2004) Interactions between BRCT repeats and phosphoproteins: tangled up in two. *Trends Biochem. Sci. 29*, 579–585.

(8) Leung, C. C., Gong, Z., Chen, J., and Glover, J. N. (2011) Molecular basis of BACH1/FANCJ recognition by TopBP1 in DNA replication checkpoint control. *J. Biol. Chem. 286*, 4292–4301.

(9) Clapperton, J. A., Manke, I. A., Lowery, D. M., Ho, T., Haire, L. F., Yaffe, M. B., and Smerdon, S. J. (2004) Structure and mechanism of BRCA1 BRCT domain recognition of phosphorylated BACH1 with implications for cancer. *Nat. Struct. Mol. Biol. 11*, 512–518.

(10) Shiozaki, E. N., Gu, L., Yan, N., and Shi, Y. (2004) Structure of the BRCT repeats of BRCA1 bound to a BACH1 phosphopeptide: implications for signaling. *Mol. Cell 14*, 405–412.

(11) Williams, R. S., Lee, M. S., Hau, D. D., and Glover, J. N. (2004) Structural basis of phosphopeptide recognition by the BRCT domain of BRCA1. *Nat. Struct. Mol. Biol. 11*, 519–525.

(12) Glover, J. N. (2006) Insights into the molecular basis of human hereditary breast cancer from studies of the BRCA1 BRCT domain. *Fam. Cancer 5*, 89–93.

(13) Rodriguez, M. C., and Songyang, Z. (2008) BRCT domains: phosphopeptide binding and signaling modules. *Front. Biosci. 13*, 5905–5915.

(14) Ekblad, C. M., Wilkinson, H. R., Schymkowitz, J. W., Rousseau, F., Freund, S. M., and Itzhaki, L. S. (2002) Characterisation of the BRCT domains of the breast cancer susceptibility gene product BRCA1. *J. Mol. Biol. 320*, 431–442.

(15) Rowling, P. J., Cook, R., and Itzhaki, L. S. (2010) Toward classification of BRCA1 missense variants using a biophysical approach. *J. Biol. Chem. 285*, 20080–20087.

(16) Nikolopoulos, G., Pyrpassopoulos, S., Thanassoulas, A., Klimentzou, P., Zikos, C., Vlassi, M., Vorgias, C. E., Yannoukakos, D., and Nounesis, G. (2007) Thermal unfolding of human BRCA1 BRCT-domain variants. *Biochim. Biophys. Acta 1774*, 772–780.

(17) Lee, M. S., Green, R., Marsillac, S. M., Coquelle, N., Williams, R. S., Yeung, T., Foo, D., Hau, D. D., Hui, B., Monteiro, A. N., and Glover, J. N. (2010) Comprehensive analysis of missense variations in the BRCT domain of BRCA1 by structural and functional assays. *Cancer Res. 70*, 4880–4890.

(18) Williams, R. S., Chasman, D. I., Hau, D. D., Hui, B., Lau, A. Y., and Glover, J. N. (2003) Detection of protein folding defects caused by BRCA1-BRCT truncation and missense mutations. *J. Biol. Chem. 278*, 53007–53016.

(19) Williams, R. S., and Glover, J. N. (2003) Structural consequences of a cancer-causing BRCA1-BRCT missense mutation. *J. Biol. Chem. 278*, 2630–2635.

(20) Carvalho, M. A., Marsillac, S. M., Karchin, R., Manoukian, S., Grist, S., Swaby, R. F., Urmenyi, T. P., Rondinelli, E., Silva, R., Gayol, L., Baumbach, L., Sutphen, R., Pickard-Brzosowicz, J. L., Nathanson, K. L., Sali, A., Goldgar, D., Couch, F. J., Radice, P., and Monteiro, A. N. (2007) Determination of cancer risk associated with germ line BRCA1 missense variants by functional analysis. *Cancer Res. 67*, 1494–1501.

(21) Karchin, R., Monteiro, A. N., Tavtigian, S. V., Carvalho, M. A., and Sali, A. (2007) Functional impact of missense variants in BRCA1 predicted by supervised learning. *PLoS Comput. Biol. 3*, e26.

(22) Tavtigian, S. V., Byrnes, G. B., Goldgar, D. E., and Thomas, A. (2008) Classification of rare missense substitutions, using risk surfaces, with genetic- and molecular-epidemiology applications. *Hum. Mutat. 29*, 1342–1354.

(23) Chasman, D., and Adams, R. M. (2001) Predicting the functional consequences of non-synonymous single nucleotide polymorphisms: structure-based assessment of amino acid variation. *J. Mol. Biol. 307*, 683–706.

(24) Mirkovic, N., Marti-Renom, M. A., Weber, B. L., Sali, A., and Monteiro, A. N. (2004) Structure-based assessment of missense mutations in human BRCA1: implications for breast and ovarian cancer predisposition. *Cancer Res. 64*, 3790–3797.

(25) Goldgar, D. E., Easton, D. F., Deffenbaugh, A. M., Monteiro, A. N., Tavtigian, S. V., and Couch, F. J. (2004) Integrated evaluation of DNA sequence variants of unknown clinical significance: application to BRCA1 and BRCA2. *Am. J. Hum. Genet. 75*, 535–544.

(26) Easton, D. F., Deffenbaugh, A. M., Pruss, D., Frye, C., Wenstrup, R. J., Allen-Brady, K., Tavtigian, S. V., Monteiro, A. N., Iversen, E. S., Couch, F. J., and Goldgar, D. E. (2007) A systematic genetic assessment of 1,433 sequence variants of unknown clinical significance in the BRCA1 and BRCA2 breast cancer-predisposition genes. *Am. J. Hum. Genet. 81*, 873–883.

(27) Kabsch, W. (1993) Automatic Processing of Rotation Diffraction Data from Crystals of Initially Unknown Symmetry and Cell Constants. *J. Appl. Crystallogr. 26*, 795–800.

(28) Mccoy, A. J., Grosse-Kunstleve, R. W., Adams, P. D., Winn, M. D., Storoni, L. C., and Read, R. J. (2007) Phaser crystallographic software. *J. Appl. Crystallogr. 40*, 658–674.

(29) Adams, P. D., Afonine, P. V., Bunkoczi, G., Chen, V. B., Davis, I. W., Echols, N., Headd, J. J., Hung, L. W., Kapral, G. J., Grosse-Kunstleve, R. W., McCoy, A. J., Moriarty, N. W., Oeffner, R., Read, R. J., Richardson, D. C., Richardson, J. S., Terwilliger, T. C., and Zwart, P. H. (2010) PHENIX: a comprehensive Python-based system for macromolecular structure solution. *Acta Crystallogr., Sect. D: Biol. Crystallogr. 66*, 213–221.

(30) Painter, J., and Merritt, E. A. (2006) Optimal description of a protein structure in terms of multiple groups undergoing TLS motion. *Acta Crystallogr., Sect. D: Biol. Crystallogr. 62*, 439–450.

(31) Painter, J., and Merritt, E. A. (2006) TLSMD web server for the generation of multi-group TLS models. *J. Appl. Crystallogr. 39*, 109–111.

(32) Emsley, P., Lohkamp, B., Scott, W. G., and Cowtan, K. (2010) Features and development of Coot. *Acta Crystallogr., Sect. D: Biol. Crystallogr. 66*, 486–501.

(33) Campbell, S. J., Edwards, R. A., and Glover, J. N. (2010) Comparison of the structures and peptide binding specificities of the BRCT domains of MDC1 and BRCA1. *Structure 18*, 167–176.

(34) Brunger, A. T. (2007) Version 1.2 of the Crystallography and NMR system. *Nature Protoc. 2*, 2728–2733.

(35) Chen, V. B., Arendall, W. B., Headd, J. J., Keedy, D. A., Immormino, R. M., Kapral, G. J., Murray, L. W., Richardson, J. S., and

Richardson, D. C. (2010) MolProbity: all-atom structure validation for macromolecular crystallography. *Acta Crystallogr., Sect. D: Biol. Crystallogr. 66*, 12–21.

(36) Baker, N. A., Sept, D., Joseph, S., Holst, M. J., and McCammon, J. A. (2001) Electrostatics of nanosystems: application to microtubules and the ribosome. *Proc. Natl. Acad. Sci. U.S.A. 98*, 10037–10041.

(37) Hess, B., Kutzner, C., van der Spoel, D., and Lindahl, E. (2008) GROMACS 4: Algorithms for highly efficient, load-balanced, and scalable molecular simulation. *J. Chem. Theory Comput. 4*, 435–447.

(38) Oostenbrink, C., Villa, A., Mark, A. E., and Van Gunsteren, W. F. (2004) A biomolecular force field based on the free enthalpy of hydration and solvation: The GROMOS force-field parameter sets 53A5 and 53A6. *J. Comput. Chem. 25*, 1656–1676.

(39) Berendsen, H. J. C., Postma, J. P. M., Vangunsteren, W. F., Dinola, A., and Haak, J. R. (1984) Molecular-Dynamics with Coupling to an External Bath. *J. Chem. Phys. 81*, 3684–3690.

(40) Essmann, U., Perera, L., Berkowitz, M. L., Darden, T., Lee, H., and Pedersen, L. G. (1995) A Smooth Particle Mesh Ewald Method. *J. Chem. Phys. 103*, 8577–8593.

(41) Darden, T., York, D., and Pedersen, L. (1993) Particle Mesh Ewald - an N.Log(N) Method for Ewald Sums in Large Systems. *J. Chem. Phys. 98*, 10089–10092.

(42) Hess, B., Bekker, H., Berendsen, H. J. C., and Fraaije, J. G. E. M. (1997) LINCS: A linear constraint solver for molecular simulations. *J. Comput. Chem. 18*, 1463–1472.

(43) Tischkowitz, M., Hamel, N., Carvalho, M. A., Birrane, G., Soni, A., van Beers, E. H., Joosse, S. A., Wong, N., Novak, D., Quenneville, L. A., Grist, S. A., Nederlof, P. M., Goldgar, D. E., Tavtigian, S. V., Monteiro, A. N., Ladias, J. A., and Foulkes, W. D. (2008) Pathogenicity of the BRCA1 missense variant M1775K is determined by the disruption of the BRCT phosphopeptide-binding pocket: a multi-modal approach. *Eur. J. Hum. Genet. 16*, 820–832.

(44) Williams, J. S., Williams, R. S., Dovey, C. L., Guenther, G., Tainer, J. A., and Russell, P. (2010) gammaH2A binds Brc1 to maintain genome integrity during S-phase. *EMBO J. 29*, 1136–1148.

(45) Stucki, M., Clapperton, J. A., Mohammad, D., Yaffe, M. B., Smerdon, S. J., and Jackson, S. P. (2005) MDC1 directly binds phosphorylated histone H2AX to regulate cellular responses to DNA double-strand breaks. *Cell 123*, 1213–1226.

(46) Lee, M. S., Edwards, R. A., Thede, G. L., and Glover, J. N. (2005) Structure of the BRCT repeat domain of MDC1 and its specificity for the free COOH-terminal end of the gamma-H2AX histone tail. *J. Biol. Chem. 280*, 32053–32056.

(47) Rodriguez, M., Yu, X., Chen, J., and Songyang, Z. (2003) Phosphopeptide binding specificities of BRCA1 COOH-terminal (BRCT) domains. *J. Biol. Chem. 278*, 52914–52918.

(48) Edwards, R. A., Lee, M. S., Tsutakawa, S. E., Williams, R. S., Tainer, J. A., and Glover, J. N. (2008) The BARD1 C-terminal domain structure and interactions with polyadenylation factor CstF-50. *Biochemistry 47*, 11446–11456.

(49) Birrane, G., Varma, A. K., Soni, A., and Ladias, J. A. (2007) Crystal structure of the BARD1 BRCT domains. *Biochemistry 46*, 7706–7712.

(50) Thanassoulas, A., Nomikos, M., Theodoridou, M., Yannoukakos, D., Mastellos, D., and Nounesis, G. (2010) Thermodynamic study of the BRCT domain of BARD1 and its interaction with the -pSER-X-X-Phe-motif-containing BRIP1 peptide. *Biochim. Biophys. Acta 1804*, 1908–1916.